Preprint Title	Suspension feeding in Copepoda (Crustacea) – introducing the first numerical model of setae action in concert
Authors	Alexander E. Filippov, Wencke Krings and Stanislav N. Gorb
Publication Date	03 März 2023
Article Type	Full Research Paper
Supporting Information File 1	Crest_3d_combined.avi; 10.6 MB
ORCID® iDs	Wencke Krings - https://orcid.org/0000-0003-2158-9806; Stanislav N. Gorb - https://orcid.org/0000-0001-9712-7953

Suspension feeding in Copepoda (Crustacea) – introducing the first numerical model of setae action in concert

Alexander E. Filippov[1,2], Wencke Krings[1,3,4,5*], Stanislav N. Gorb[1]

[1]Department of Functional Morphology and Biomechanics, Zoological Institute, Christian-Albrechts-Universität zu Kiel, Am Botanischen Garten 1–9, 24118 Kiel, Germany

[2]Donetsk Institute for Physics and Engineering, National Academy of Sciences of Ukraine, 83114 Donetsk, Ukraine

[3]Department of Behavioral Biology, Institute of Cell and Systems Biology of Animals, Universität Hamburg, Martin-Luther-King-Platz 3, 20146 Hamburg, Germany

[4]Department of Mammalogy and Paleoanthropology, Leibniz Institute for the Analysis of Biodiversity Change, Martin-Luther-King-Platz 3, 20146 Hamburg, Germany

[5]Department of Cariology, Endodontology and Periodontology, Universität Leipzig, Liebigstraße 12, 04103 Leipzig, Germany

*corresponding author: wencke.krings@uni-hamburg.de

Abstract

Suspension feeding by particle collecting setae is common within Crustacea. Even though the mechanisms behind it and the structures themselves were studied for decades, the interplay between the different setae types and the parameters contributing to their particle collecting capacities remain enigmatic. Here, we provide a numerical model approach to understand the relationship between mechanical property gradients, mechanical behaviour, adhesion of the setae and the feeding efficiency performed by the system. We constructed the first simple dynamic numerical model, which interacts with the food particles and delivers them into the mouth opening. By altering the parameters, it was unraveled that the system performs best, if the long and short setae have different mechanical behaviour and different degrees of adhesion, since the long setae generate the feeding current and the short ones establish the contact with the particle. This protocol can be applied to any system in the future, as the parameters (properties of particles and setae, arrangement, etc.) can be easily

altered. This will shed light on the biomechanical adaptations of this feeding structure to suspension feeding and provide inspiration for biomimetics in the field of filtration technologies.

Keywords

Feeding structure; CLSM; mechanical properties; feeding efficiency; adhesion

Introduction

Particle capture mechanisms can be found in a huge variety of aquatic animals as e.g. polychaetes, bryozoans, bivalves, sponges, echinoderms, cnidarians, or crustaceans [see e.g., 1, 2, 3, 4, 5, 6, 7]. Even though living conditions and bauplans differ highly between suspension feeders, there are two main mechanisms for particle collection from the water body [for throughout review on suspension feeding, see 8, 9, 10, 11]. The first one can be described as filtering or sieving with e.g., setae, cilia, or mucous nets, and is present in form of passive or active suspension feeding. Passive feeders rely on external water currents that bring food particles to the filtering structures and active feeders create a feeding flow by pumping systems. The second mechanism involves water flow manipulating structures (setae, tentacles, etc.) that redirect the food particles and lead them to specialized structures, which contact and capture them. A good example using the latter mechanism are the filtering setae of crustaceans [for throughout reviews, see 12, 13]. Even though most crustaceans are primarily raptorial, suspension-feeding plays an important role. In general, the feeding current is generated by multiple pairs of appendages and the particles are captured by plumate “filter setae”, which cover the trunk and head appendages. These setae have to establish a contact with the particles by inertial impaction, capture and transport them to the mouth opening [see e.g., 14, 15, 16, 17, 18].

These interactions (i.e., making contact, handling or manipulation of particles, etc.) were previously documented detailly, as it can be observed under binocular microscope [see e.g., 19, 20, 21, 22, 23, 24, 25, 26, 27, 28]. In this context, the setae morphology and mesh size of the filtering structure, the surface chemistry and forces (e.g., Van der Waals forces) of feeding structures and particles – especially when the particles are of smaller diameter than the meshes of the sieve – are of high importance [see

54 e.g., 14, 29, 30, 31, 32, 33, 34, 35, 36]. Additionally, the mechanical property gradients of the setae,
55 with soft bases or soft tips, seem to play a role [25, 37, 38].
56
57 All of the above-mentioned parameters influence the setae capability to capture and transport the
58 particles – but to which extend is unknown, since these parameters cannot be manipulated in the living
59 organisms. To test how feeding efficiency depends on the mechanical property gradients and the
60 adhesion forces of the setae, we here present the first numerical model, which simulates the interplay
61 between setae during suspension feeding. As model organism we chose the copepod *Centropages*
62 *hamatus* (Lilljeborg, 1853). This species belongs to the Calanoida, where filter feeding is the derived
63 condition [see e.g., 19, 20, 29, 39, 40, 41, 42, 43, 44, 45, 46, 47, 48, 49, 50, 51]. In this species (Figure
64 1), previous confocal laser scanning microscopy (CLSM) studies on the cuticle's mechanical properties
65 revealed, that the setae on the maxilla 1 (long setae) and 2 (short setae) possess very soft bases full of
66 the elastic protein resilin [52, 53, 54]. Additionally, the tips from the short setae on maxilla 2 exhibited
67 a blue autofluorescence signal, which strongly indicated that these tips are also rather soft and flexible,
68 similar to attachment hairs in insects showing high adhesion at the tips [see e.g., 55; for throughout
69 reviews, see 56, 57, 58]. In contrast, the tips of the long setae did not emit blue signals.

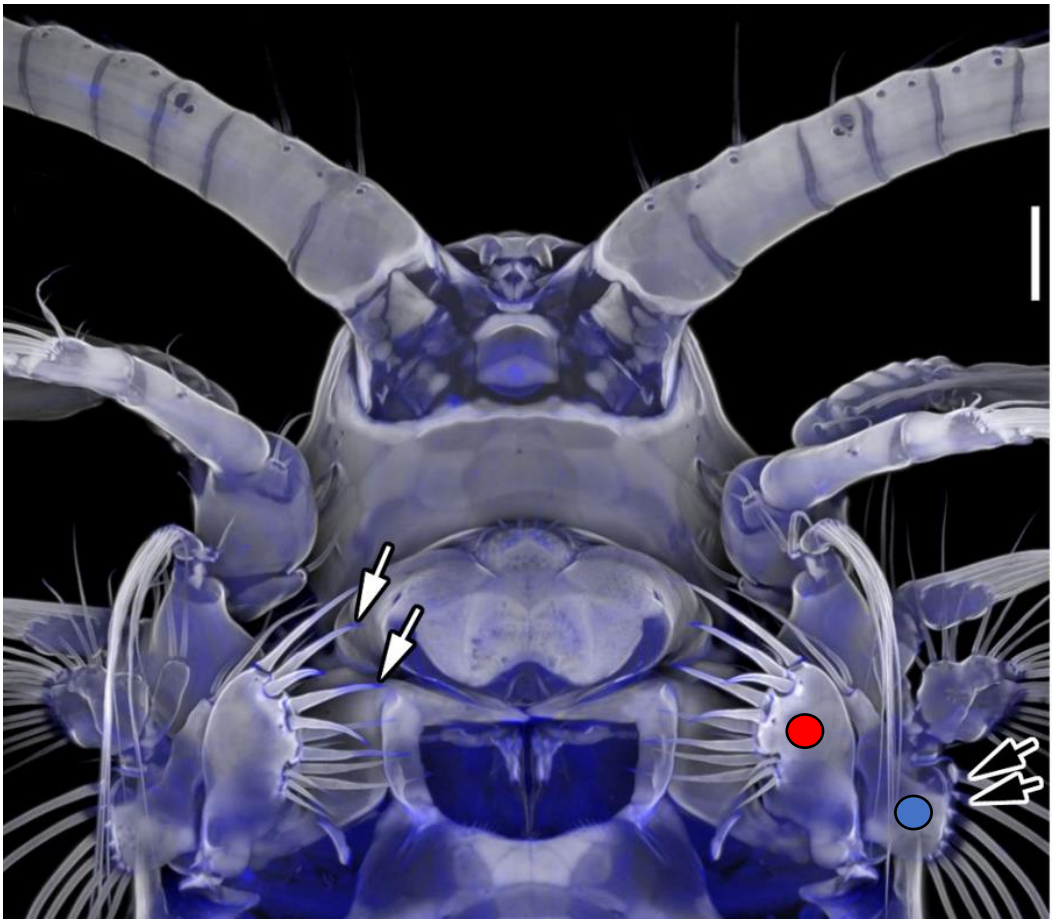

Figure 1. Confocal laser scanning micrograph (maximum intensity projection) showing the exoskeleton of a female copepod crustacean *Centropages hamatus* in ventral view. The black arrows highlight the outer long setae with resilin occurrence at their bases and the white ones the setae with resilin occurring at their tips. The red circle highlights maxilla 1 and the blue one maxilla 2. Scale bar on right side = 50 µm. Figure 1 was adapted (by adding arrows and circles) from [54], J. Michels, "Confocal laser scanning microscopy – detailed three-dimensional morphological imaging of marine organisms", Imaging Marine Life, with permission from John Wiley and Sons. Copyright © 2014 Wiley-VCH Verlag GmbH & Co. KGaA. This content is not subject to CC BY 4.0.

The here presented simulation took the actual physical processes of the water body (interplay between particles, etc.) into account. Two types of setae (long and short ones) were arranged on crests, similar to the real situation in the copepods, and their parameters (adhesion, mechanical property gradients) altered. These models produced data on the effectivity of particle collection, the particle motion

patterns, and the transfer of particles to the mouth opening. It clearly depicts that short and long setae are more effective, when they work in concert, have different mechanical properties and different adhesion forces. Based on this study, which is rather a protocol for carrying out more extensive numerical modelling in the future, the model can be easily computed with MatLab and the parameters of the model (e.g., the size of the food particle, the quantity and mechanical properties of setae, etc.) can be adjusted to the specific system or problem. This model shall serve as a basis to unravel the interplay between the suspension feeders feeding structures, the preferred food, and the gathering performance.

Additionally, it could open new avenues in the development of new filtration technologies (e.g., mucus-like filter media, bioinspired membranes) that use adhesive forces to retain particles. In contrast to organisms, which collect particles at nano- to millimeter scale, most industrial cross-flow filtration systems can capture material in a smaller size range – highlighting the necessity of investigating particle retention in biological systems.

Experimental

Specimens studied

As a model organism we chose *Centropages hamatus* (Crustacea, Copepoda, Calanoida). The mechanical properties of the setae were previously documented by CLSM [52, 53, 54]: the short setae on maxilla 2 possess soft tips and soft bases and the long setae on maxilla 1 only soft bases (Figure 1).

Mathematical model

For the simulation we employed MatLab R2022a (The MathWorks, Inc., Natick, Massachusetts, USA). Our discrete numerical model described the dynamics of two pairs of initially parallel aligned elastic crests, resembling the maxillae. The conceptual structure of the model is depicted in Figure 2. The dynamic behavior of the model can be found in the Supplementary movie.

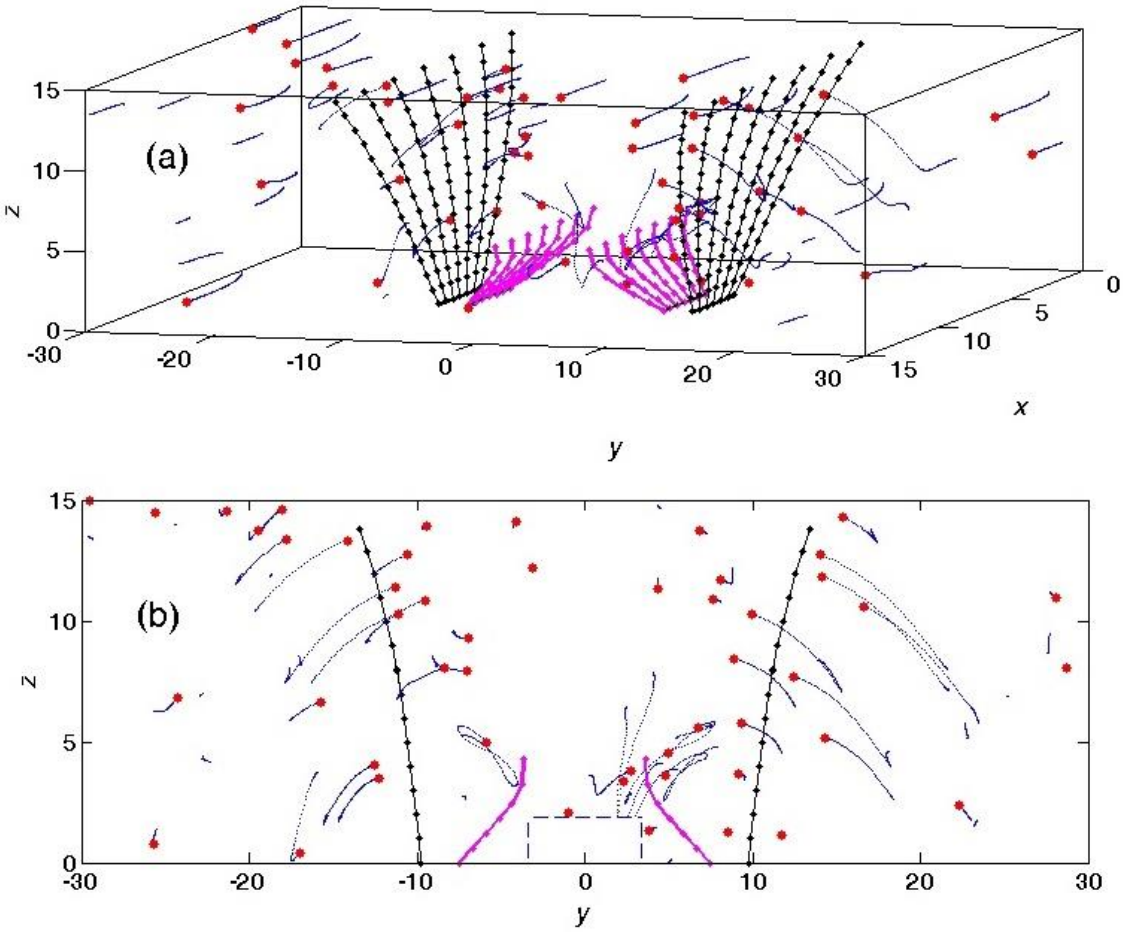

Figure 2. Conceptual structure of the numerical model. Setae, arranged as two pairs of setae rows (internal short setae and external long setae) were simulated by lines with small circles. Each small circle separated two elastically connected seta segments. The big red circles represented the instant position of the movable particles ("food"). The dotted comet tails behind each particle visualized small fragments of particle trajectories. (a) shows the 3-dimentional view on the system and (b) its projection on the plane (z,y). The mouth opening was simulated as dashed line box.

Each seta was constructed of a number of elastic segments, each having the same length dR. The segments were provided with longitudinal ($K^{||}$) and transverse ($K^{\perp}$) stiffness, $K^{||} = K^{\perp}$. The transverse stiffness tended to hold the angle between the neighboring segments close to 180°. According to the goals of this study we varied the stiffness from segment to segment depending on the hypothetical particular structure.

A deformation of the setae produced elastic forces proportional to the seta stiffness. The forces were described by the following equations:

$$\vec{F}_{jk}^{||} = K^{||}(\vec{R}_j - \vec{R}_k)\left[1 - \left(\frac{\vec{R}_j - \vec{R}_k}{dR}\right)^2\right], \text{ and } \vec{F}_j^{\perp} = K^{\perp}(2\vec{R}_j - \vec{R}_{j+1} - \vec{R}_{j-1}) \quad (1)$$

where $\vec{R}_j$ was a position vector of the middle of the segment (the node) *j*; $k = j \pm 1$. The longitudinal force, $\vec{F}_{jk}^{||}$, was described here by a double-well potential, which tended to keep a distance between the nodes $\vec{R}_j$ and $\vec{R}_{j\pm1}$ close to the equilibrium length of each segment dR.

This particular form of the longitudinal force equation was chosen, because it is linear at small displacement and increases non-linear at large displacement. The transverse force, $\vec{F}_j^{\perp}$ was directly proportional to the lateral deflection and tended to keep the position $\vec{R}_j$ close to the mean value between its nearest neighbors, $(\vec{R}_{j+1} + \vec{R}_{j-1})/2$. Additionally, it kept the direction of every segment as close to parallel with the adjacent ones as possible – at current balance of all the forces. The transverse force in the present form was easy to realize numerically, but it was not purely bending force, since this may include a longitudinal component.

In the model, each long seta was constructed with 15 segments and each short one with 7 segments. Each seta was rotated around a base segment from minimal to maximal angles, $\varphi_{\min}$ and $\varphi_{\max}$ respectively. We varied these angles in wide interval to simulate the different rotational mobility of the individual long and short seta. Angle speed (frequency of the rotation in both directions) was also widely varied for each seta.

The food was represented by an array of $N_p = 50$ particles, moving in 3-dimentional space with periodic boundary conditions. The particles were created following established protocols [59, 60, 61, 62, 63, 64]. For all the results, presented below, the number $N_p = 50$ was fixed as a compromise between statistically representative value and time consumption of the calculations.

It was supposed that every particle interacts viscously with a "water flow", caused by both external flow and motion of the setae. Initially, the particles were placed randomly in a box $[0, L_x\,; -L_y, L_y\,; 0\,, L_z]$ and their velocity was equal to the velocity of external "water flow" v_{ext}. If any particle leaved the box, it was randomly injected back to the system with the same velocity. The same was also done in the case of the particle being "eaten". The particle was treated as "eaten" when it appears inside the region "mouth", which was represented by a small box in the center of ground plane with rectangular (parallelepiped) borders: $[0, L_{mouth,x}\,; -L_{mouth,y}, L_{mouth,y}\,; 0\,, L_{mouth,z}]$.

Being separated by water, the particles moved practically independently one from another. So, particles did not interact with another one in our model directly. However, each particle interacted with the setae via the liquid. Due to strong damping, each particle tended to equilibrate its speed with the local velocity of the liquid. This velocity, in turn, was determined by a combination of the external flow v_{ext} and perturbations, caused by the motion of the setae.

Appropriate force acting on every particle from the setae could be represented as a combination of the following velocity and distance depending factors:

$$f_{kj} = \Theta(\vec{r}_k - \vec{r}_j)\Phi(\vec{v}_k - \vec{v}_j). \quad (2)$$

Here, the first factor described the tendency to equilibrate the velocities of every particle and each segment of the seta. The second one determined, how this interaction decays with instant distance between the particle and segment. As a first approximation, one can accept that these factors linearly depended on the difference between the velocities, and exponentially decreased with the distance in phase (speed, velocity) space $\{v, r\}$ between the chosen particle and each segment:

$$\Theta(\vec{r}_k - \vec{r}_j) \sim exp(-|\vec{r}_k - \vec{r}_j|/r_0); \Phi(\vec{v}_k - \vec{v}_j) \sim (\vec{v}_k - \vec{v}_j)\, exp(-|\vec{v}_k - \vec{v}_j|/v_0)\, \Theta(\vec{r}_k - \vec{r}_j). \quad (3)$$

As it was mentioned, the particles were involved in the water motion. Thus, same velocity depending interaction existed between the particles and the external flow of water. It can be written in this form:

$$\Phi_{ext}(\vec{v}_k - \vec{v}_{ext}) \sim (\vec{v}_k - \vec{v}_{ext})\, exp(-|\vec{v}_k - \vec{v}_{ext}|/v_0)\, \Theta(\vec{r}_k - \vec{r}_j). \quad (4)$$

Besides the equilibration of the velocities, there is a direct mechanical (or chemical) interaction between the setae and the particles. Especially, this interaction becomes important for the thin elastic ends of the short setae near the mouth opening. In particular, the adhesion by Van der Waals attraction becomes possible at such scales. This part of the interaction must also be included in the model; in a form of potential interaction between the setae (their tips) and the food particles.

Corresponding force could be written in the following gradient form:

$$f_{VdW}(\vec{r}_k - \vec{r}_j) = -\frac{\partial U_{VdW}(r)}{\partial r}(\vec{r}_k - \vec{r}_j)/\left|\vec{r}_k - \vec{r}_j\right|, \quad (5)$$

where for definiteness $U_{VdW}(r)$ and minimization of the numerical calculations could be represented by relatively simple Morse potential $U_{VdW}(r) = U_0(1 - exp(-a(r - r_{VdW})))^2$.

The combined influence of all the forces, mentioned above, led to a typical dynamic scenario, which is recorded in the Supplemented movie. It quite realistically reproduced the behavior of particles moving around a real animal (see e.g., https://www.youtube.com/watch?v=5RZwLbRd3b4).

It is important to note, that due to randomness in the initial conditions and the injection of "eaten" particles back into the system, the particular feeding sequences never repeated one another exactly. However, after a short transient period, a well-defined quasi-periodic ("strange attractor") motion self-organized in the system, which could be easily analyzed statistically. Besides, one could vary the parameters of the model equation and receive similar behaviors.

Numerical simulations

In this study we restricted ourselves to a few biologically important questions:

1. Is there a difference in feeding performance between a system, possessing only short setae near the mouth opening, and a system with both types of setae, long and short ones?

2. Which mechanical parameters (flexible or stiff) of the setae segments facilitate the feeding of particles?
3. How does the feeding efficiency change when the setae tips have a high adhesion?
4. How does the feeding efficiency change when the basic segments of each setae are more flexible and allows a higher bending amplitude?

To elucidate this, we performed a set of numerical simulations with different configurations of the setae, the segments' elasticity and the adhesion of the segments.

The relationship between different variants of the elasticity for a system, composed of only short setae, as well as for a system, containing short and long setae, and the number of eaten particles was summarized in the Figures 3–6.

Figure 3 represents the time dependencies of $N_{eaten}(t)$ for 4 different variants of the **short setae**:

2) soft setae, without high adhesion at tips;

3) hard setae with soft tips, without high adhesion at tips;

4) hard setae, without high adhesion at tips;

5) hard setae with soft tips and high adhesion at tips. This configuration led to the consumption of most particles.

These variants were numbered respectively in the Figure 3. For comparison, we also included a curve (line 1 in Figure 3), which depicts the number of eaten particles $N_{eaten}(t)$ in a system without setae. Here, only the flow of water randomly transported some particles to the mouth opening and caused some slow accumulation of $N_{eaten}(t)$.

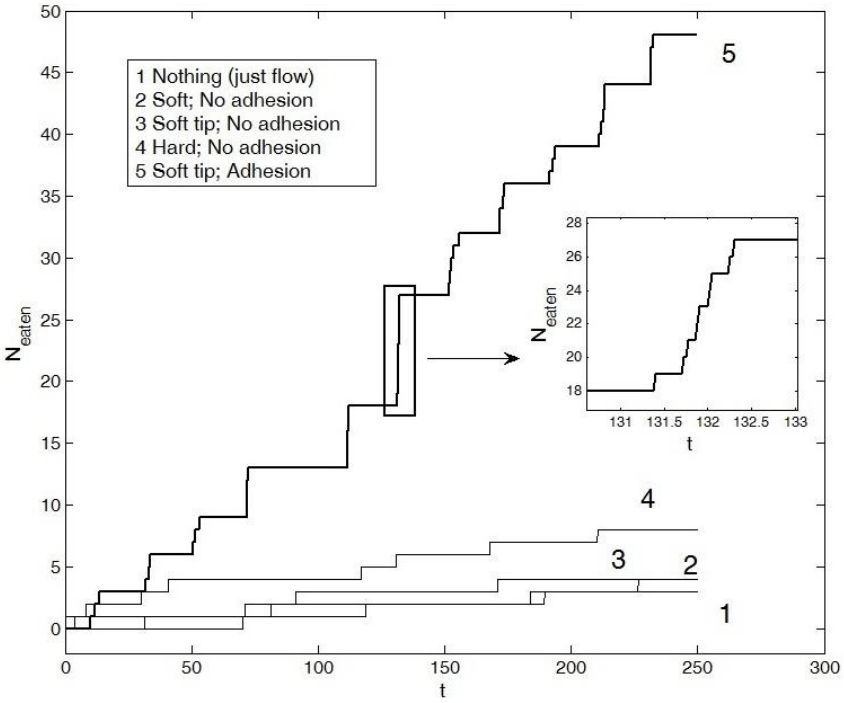

Figure 3. Number of eaten particles over time for the system containing only short setae (lines 2–5). Line 2 corresponds to a system with soft setae without high adhesion at tips; line 3 to hard setae with soft tips, without high adhesion at tips; line 4 to hard setae, without high adhesion at tips; line 5 to hard setae with soft tips and high adhesion at tips. Line 1 corresponds to the reference system, which does not contain setae at all (food particles are transported into the mouth by water motion). The insert depicts the fine structure of one typical big step corresponding to an avalanche of the eaten particles during relatively short time interval. The characteristic time intervals between the avalanches correlate with the periodic oscillations (rotations) of the system. The bold curve highlights the optimal configuration (hard setae with soft tips and high adhesion at tips).

It is important to note, that the large steps on the curves were not caused by the accuracy of the calculation, but appeared only as an “optical illusion” due to presentation of the figure in limited size. In fact, each step was a consumption avalanche, which appeared quasi-periodically during long time run. At appropriate magnification, every large step on the curve had a fine structure with plenty of small steps. Due to the limit of the small accumulation window (coinciding with elementary time interval of actual calculation), every such step could be resolved down to the independent

consumption of the sole particle. This fine structure was illustrated for one of the typical avalanches in Figure 3.

Analogous dependencies $N_{eaten}(t)$ were then plotted in Figure 4 for the system with both **short and long setae**. For this scenario, we chose the optimal case from the previous scenarios (hard short setae with soft tips and high adhesion at tips, highlighted with a bold line in Figure 3) as a reference curve (number 1) in Figure 4. For the long setae we have chosen the setup without adhesion at their tips. We simulated the following scenarios for long setae:

2) hard setae (this configuration led to the consumption of most particles);

3) soft setae;

4) hard setae with soft tips.

All cases were numbered in the Figure 4. It can be directly seen, that line 2 corresponded to the maximal $N_{eaten}(t)$. As before, this optimal case was highlighted by a bold line in Figure 4 and some typical avalanches were magnified in Figure 4.

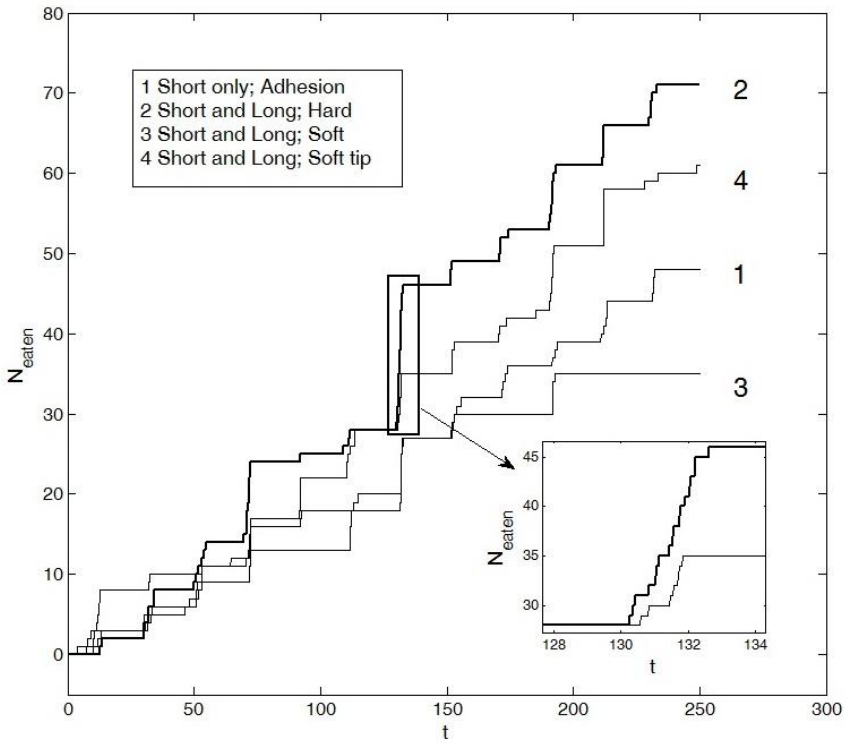

Figure 4. The same as in the Figures 3, but for the system containing both long and short setae. Line 1 corresponds to the optimal configuration of short setae, taken from the previous figure (hard short setae with soft tips and high adhesion at tips; line 5 in Figure 3). For the long setae, no adhesion was chosen. Lines 2–4 correspond to the configurations, where short setae had the optimal and same properties and the long setae were varied: line 2 depicts the quantity of ingested particles by hard long setae without adhesion at their tips; line 3 by soft long setae with high adhesion at their tips; line 4 by hard setae with soft tips without adhesion at their tips. The insert shows a small-time interval with visually resolved avalanches. Different time intervals between larger steps with different heights correspond to random mutual correlations in motion of the short and long setae. The optimal configuration (line 2) with hard long setae without adhesion at their tips is highlighted by a bold line.

The previous CLSM images revealed, that the long setae do not exhibit a blue autofluorescence and that there is most likely no adhesion on the tips present. To however test, if adhesion on these setae would influence the feedings capacity, we varied the degree of adhesion for this type. Figure 5 represents the time dependencies of $N_{eaten}(t)$ for 3 different variants of the **long setae**:

1) without adhesion at tips;

2) with strong adhesion at tips;

3) with intermediate adhesion at tips. This configuration led to the consumption of more particles, because, due to adhesion, food particles followed the setae and came to the vicinity of the mouth, where short ones collected them and transported them into the goal. However, when the adhesion was too strong, the food particles continued to follow the setae, even after their appearance in the vicinity of the short setae, and almost never entered the mouth.

We additionally altered the degree of adhesion more detailly and performed multiple experiments (see Figures 5–6 and captions to them). From these experiments it became quite obvious, that there was an optimal degree of adhesion for the long setae which supported the system. If adhesion was

present in the real structure by surface forces should be investigated in the future by either high resolution CLSM images or by employing atomic force microscopy.

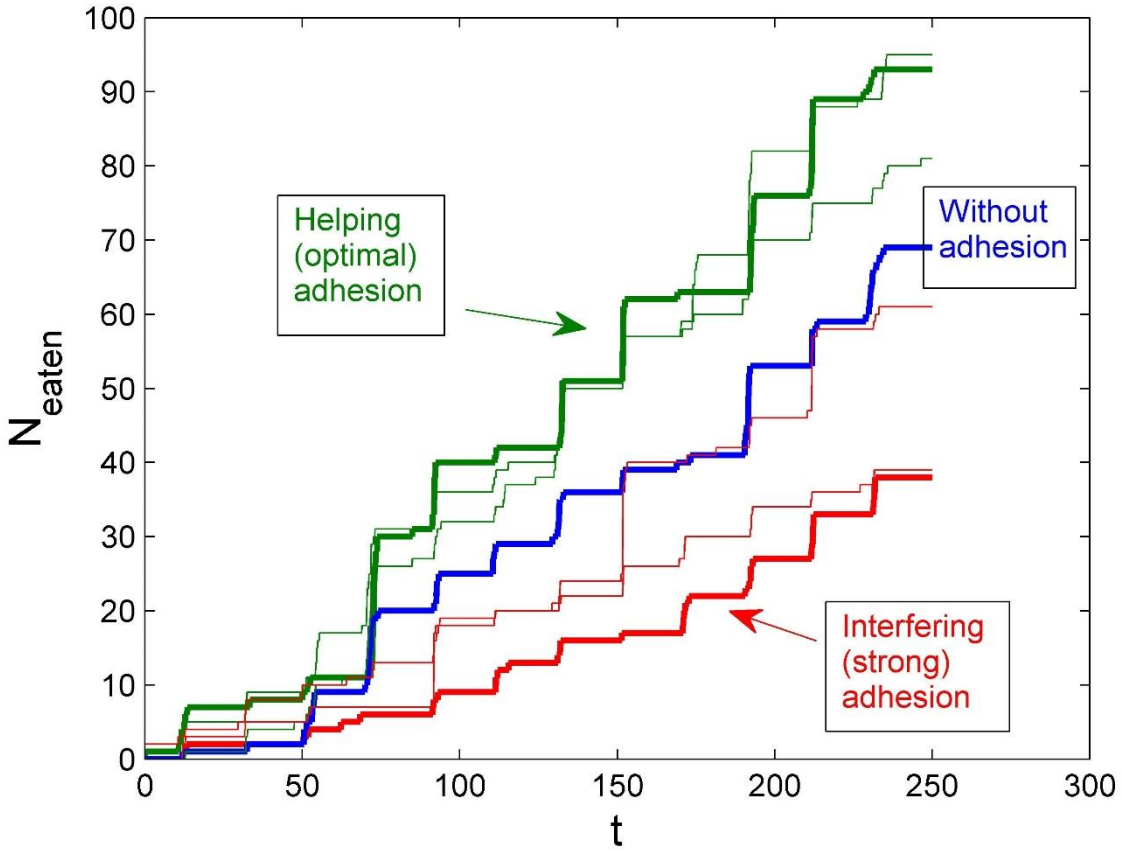

Figure 5. Number of eaten particles over time for the system containing both short and long setae, where nonzero adhesion of the long setae also exists. All other parameters are the same as were optimized for the system without adhesion of the long setae. The blue line corresponds to a system with setae without adhesion at their tips; the red line to setae with strong adhesion at their tips; the green line to setae with intermediate adhesion at tips. The green curve represents the optimal configuration.

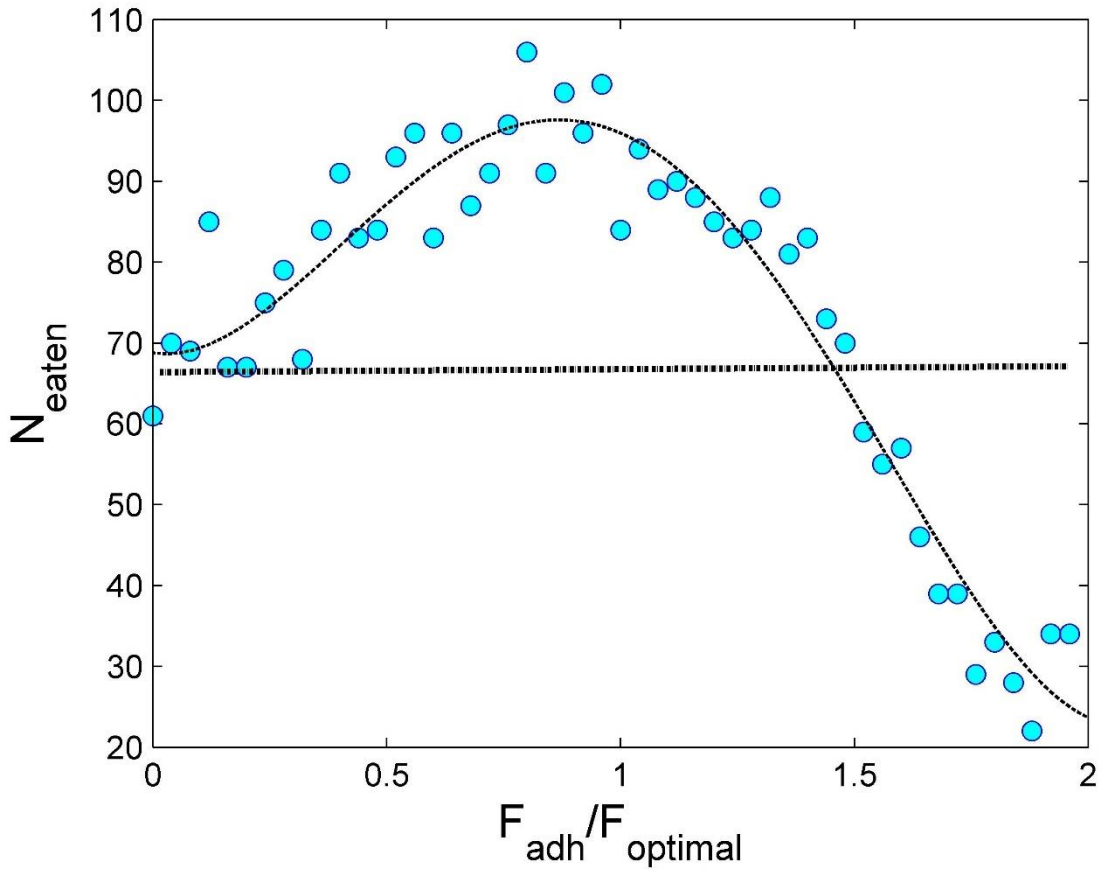

Figure 6. Number of eaten particles for different degrees of adhesion for the long setae tips. Multiple experiments were performed. Each blue circle here corresponds to the final number $N_{eaten}(t)$ obtained at the end $t = 250$ of long-time run analogous to the presented in the previous figure at random initial configuration of the food particles and varied step by step adhesion force. It is obvious that at intermediate adhesion most particles were eaten, but when the adhesion was too strong, they could not be transported into the mouth opening. If and to which extend long setae have adhesion on their tips in real copepods awaits further investigations.

As it was visualized by CLSM, the basal parts of some short and long setae appear to be relatively soft. This should influence the mobility of the rotating setae. To check this in numerical simulations, one can integrate an angle to which every seta can rotate to the mouth, $\varphi_{\min}$.

As above, for the beginning, we excluded the long setae and only simulated the system with the short setae (with the optimal configuration, i.e., with soft adhesive tips). The results of this procedure were summarized in Figure 7.

As seen directly from the plots, the well pronounced threshold angle was $\varphi_{\min} = -0.375\pi$. Below this threshold, there was practically zero consumption of the system. Paradoxically, the quantity of ingested particles was even smaller than in the pure reference system without the setae (just flow of water). Visual observation of the behavior in simulations showed, that when the absolute value of $\varphi_{\min}$ was smaller than the critical one, short setae couldn't get inside the mouth opening. Instead, they caught surrounding particles and permanently moved them back and forth ("screening"). As result, they practically blocked the mouth entrance.

It was also found, that the particular angle $\varphi_{\min} = -0.4\pi$ is very close to an optimum. This value was actually used for all the simulations presented in the previous Figures 3–6, and to record the movie in the Supplementary.

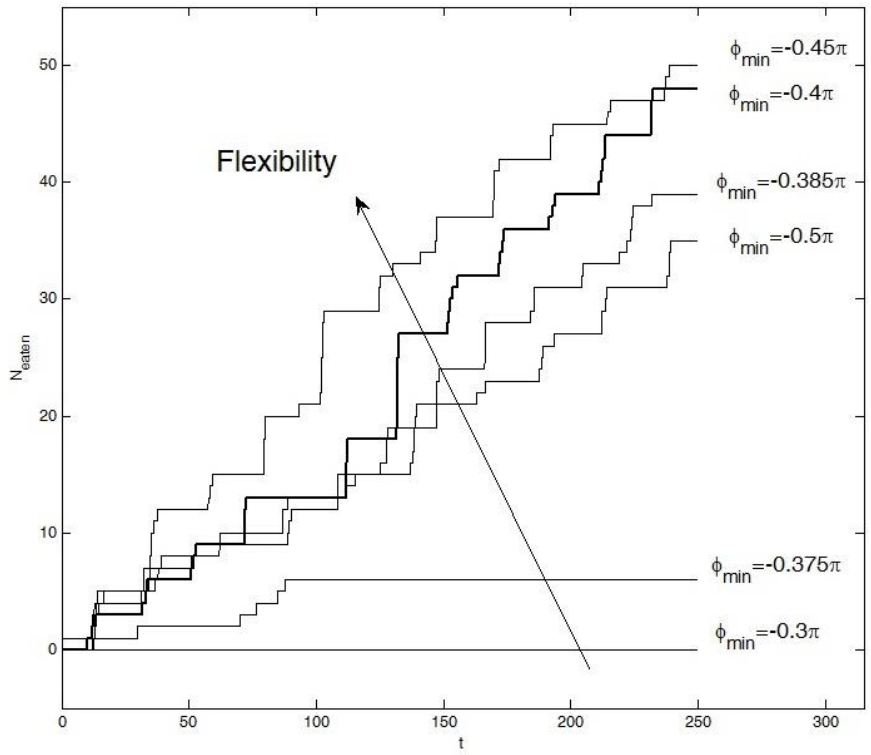

Figure 7. Time dependencies of N_{eaten} at different angles of rotation for the basic segments of the short setae. The threshold angle, around $\varphi_{\min} = -0.375\pi$, at which the system stopped delivering particles into the mouth opening is easily identified. The optimum $\varphi_{\min} = -0.4\pi$ is highlighted with a bold line and was used for all previous simulations.

The same calculations were done for a system, containing short and long setae. The results are shown in the Figure 8. It is important to note, that the angle $\varphi_{\min} = -0.5\pi$ (here, the basic segments runs parallel to the surface $z = 0$) is worse than $\varphi_{\min} = -0.4\pi$, which was the optimal one.

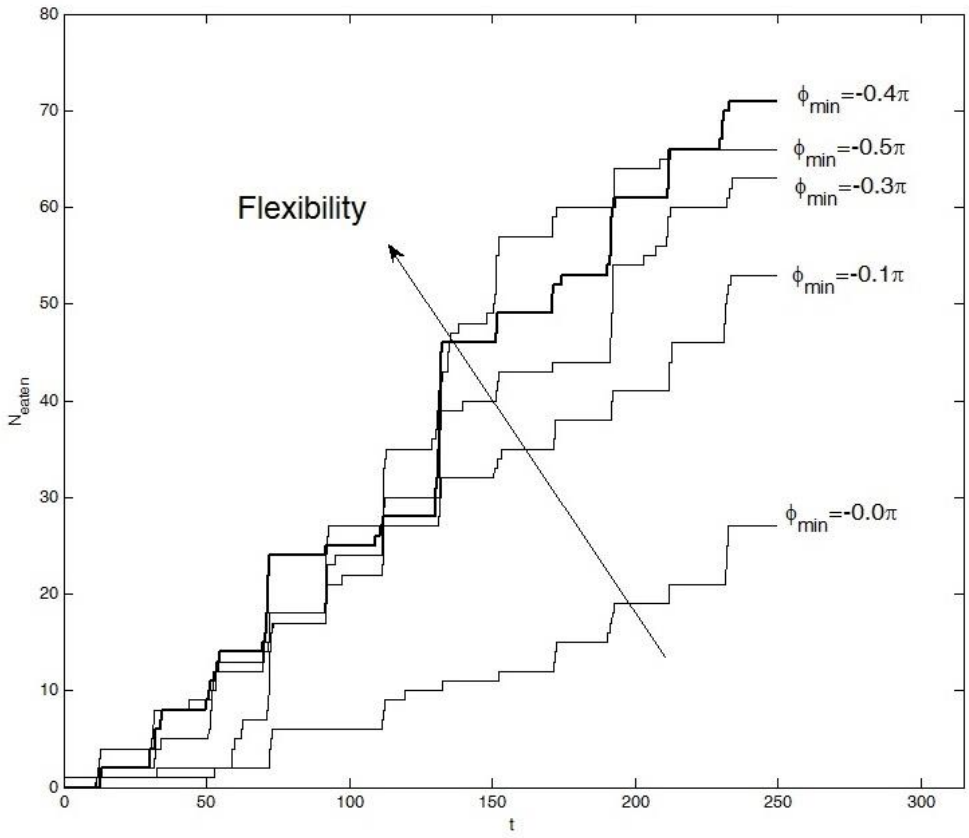

Figure 8. The same as in Figure 7 for the system containing both long and short setae. The short setae had the optimal fixed angle of rotation $\varphi_{\min} = -0.4$; the angle of rotation for the long ones was varied. The curve corresponding to the optimal angle is highlighted by a bold line.

335 The dynamic behavior of the systems with different parameters could be presented in static form by
336 density portraits projected on $\{z, y\}$ plane and histograms of distribution along the y axis, accumulated
337 during long runs. Figures 9 and 10 present the results of such an accumulation for four cases with
338 extremely different behaviors. Darker color in the grayscale maps corresponded to a higher food
339 particle density. Thin curves represented the instant particles and the bold curves the histograms
340 averaged over time, respectively.
341
342 Subplots in Figure 9 illustrate the particle distributions for the short setae with (a, c) and without
343 adhesion (b, d). The first pair of the subplots (a, c) clearly demonstrate what happens during the
344 "screening" action described above, which appeared when the rotation angle was smaller than the
345 critical one and the seta did not allow particles to enter the mouth opening. One can see very dark
346 regions in the map, where particles spent main time, following the periodic rotation of the setae
347 without entering inside the "mouth opening". The corresponding histogram integrated over time and
348 vertical direction transparently confirmed particle localization in a small region. It even reproduced
349 well pronounced maximums near so-called "stopping points", where the rotation changes direction.
350 In these places, particles, due to inertia, left, for a short time, the closest proximities of the setae tips,
351 but were very soon attracted to them again.
352 The second pair of the subplots (b, d) shows, that particles were much wider dispersed when the
353 system lacked adhesion. In this case, particles entered the mouth from time to time, but many of their
354 trajectories still led into the "wrong direction". As result, the particles periodically repeated a lot of
355 "parasitic" oscillations before final entering the mouth.
356

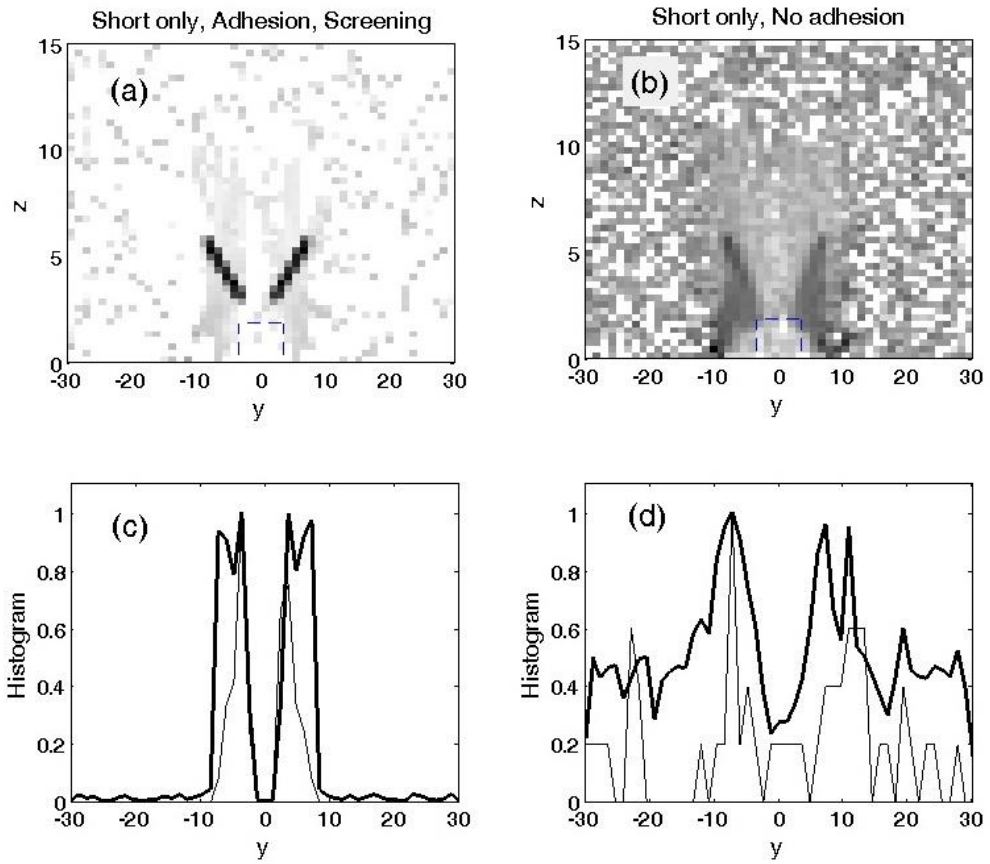

357

358 **Figure 9.** Density distributions accumulated during long-time runs on $\{z, y\}$ plane shown by grayscale
359 maps, which were normalized to the density maximums and the corresponding histograms, integrated
360 additionally over z -axis. The darker color corresponds to a higher density of particles. The thin curves
361 represent instant histograms and the bold ones the particles averaged over time. Subplots (a)-(c) and
362 (b)-(d) illustrate the particle distributions for the short setae with and without adhesion. "Screening"
363 actions (a, c) means, that the rotation angle was smaller than the critical one, and that the setae
364 practically did not allow particles to enter the mouth.

365

366 The plots in Figure 10 reproduce the results of two mostly optimal configurations, found above, for a
367 system only containing short setae (optimal case: with adhesion at their tips) and for the system
368 containing long and short setae (short setae: with adhesion at their tips; long setae: hard without
369 adhesion on their tips; rotation angle: $\varphi_{\min} = -0.4\pi$). They are depicted in the pairs of subplots (a)-
370 (c) and (b)-(d), respectively. The smooth gray areas correspond to the regions with good statistics,
371 where plenty of the particles were accumulated efficiently by the rotation of the setae and quickly

move into the mouth. The black spots on the left and right sides of the mouth show the places where particles accumulated with time, but couldn't enter to the mouth and quasi-periodically oscillate during long time. The difference in accumulation for these two cases is obvious and highlights that a system containing both setae types (b, d) is optimal for gathering particles from the surrounding water.

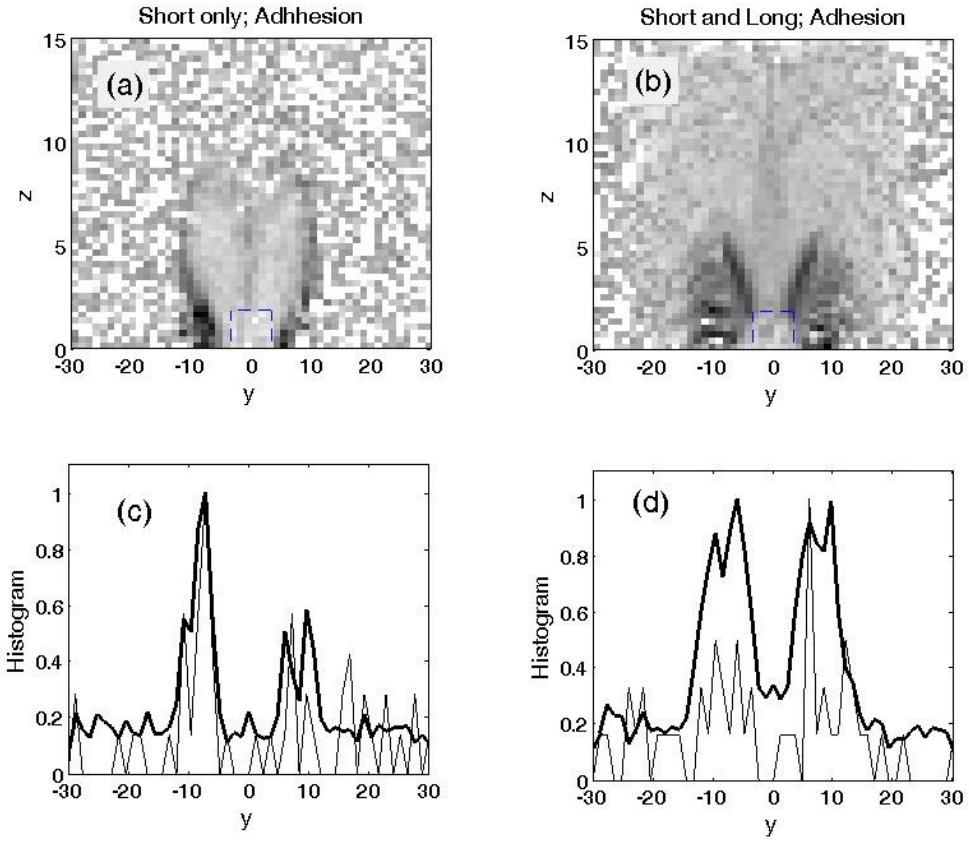

Figure 10. The same as in Figure 9 for two optimal configurations: (a, c) with only short setae (hard setae with soft tips and high adhesion at tips) and (b, d) with long setae (hard with no adhesion at their tips) and short setae (hard with soft tips and high adhesion at tips). Smooth gray areas correspond to the regions with good statistics, where plenty of the particles were accumulated and were quickly moved into the mouth. Black spots on the left and right sides of the mouth show the places where particles accumulate over time but couldn't enter the mouth. Difference in accumulation for these two cases can be directly seen; (b, d) can be identified as the optimal configuration to collect particles from the surrounding water.

Conclusion

We here present the first numerical model of the feeding setae of crustacean, taking the actual physical processes of the environment into account. It estimates the particle collecting efficiency depending on the mechanical property gradients and the adhesion of the different setae. Following this protocol, the model can be easily extended with adjustment of the parameters to fit the specific suspension feeding system or different food items. It also could serve as an inspiration to develop new filtering techniques with adhesive elements retaining particles from micro- to millimeter scale.

Supporting information. Supplementary movie. It shows the dynamic behaviour of the model.

Author contribution. AF created the numerical model. AF and WK wrote the first draft of the manuscript. SG initiated and designed the study.

Acknowledgements. We would like to thank the reviewers for their supportive comments.

Competing interests. The authors declare no competing interest.

Funding. This research was financed by the DFG grant KR 5540/2-1 to WK and Alexander von Humboldt Alumni Fellowship UKR 1118826 GFPR to AEF.

Data availability statement. All data can be found either in the paper or in the Supplementary movie.

Ethics approval statement. Not applicable.

Patient consent statement. Not applicable.

Permission to reproduce material from other sources. Not applicable.

Clinical trial registration. Not applicable.

References

1. Jørgensen, C. B. *Biology of suspension feeding;* Pergamon Press: Oxford, 1966.
2. Jørgensen, C. B. *Annu. Rev. Physiol.* **1975**, 37, 57–79.
3. Strathmann, R. R. Larval feeding. In *Reproduction of marine invertebrates. Vol. IX. General aspects: seeking unity in diversity;* Giese, A. C.; Pearse, J. S.; Pearse, V. B., Eds.; Blackwell Scientific Publications: Palo Alto, CA, 1987; pp 465–550.

4. Wotton, R. S. Methods for capturing particles in benthic animals. In *The biology of particles in aquatic systems;* Wotton, R. S., Ed.; Lewis Publishers: Boca Raton, FL, 1994; pp 183–204.
5. Riisgård, H. U.; Larsen, P. S. *Biol. Rev. Camb. Philos. Soc.* **1995**, 70, 67–106.
6. Riisgård, H. U.; Larsen, P. S. *Limnol. Oceanogr.* **2000**, 45, 1192–1195.
7. Riisgård, H. U.; Larsen, P. S. *Limnol. Oceanogr.* **2001**, 46, 882–891.
8. Hentschel, B. T.; Shimeta, J. Suspension feeders. In *Encyclopedia of Ecology;* Jørgensen, S. E.; Fath, B. D., Eds.; Academic Press, 2008; pp 3437–3442.
9. Riisgård, H. U.; Larsen, P. S. *Mar. Ecol. Prog. Ser.* **2010**, 418, 255–293.
10. Kiørboe, T. *Biol. Rev.* **2011**, 86, 311–339.
11. Hamann, L.; Blanke, A. *J. R. Soc. Interface* **2022**, 19, 20210741.
12. Garm, A.; Watling, L. Chapter 6. The crustacean integument: setae, setules, and other ornamentation. In *The Natural History of the Crustacea, Volume 1;* Thiel, M.; Watling, L., Eds.; Oxford University Press, 2015; pp 167–198.
13. Riisgård, H. U. Chapter 15. Filter-feeding mechanisms in crustaceans. Lifestyles and feeding biology. In *The Natural History of the Crustacea, Volume 2;* Thiel, M.; Watling, L., Eds.; Oxford University Press: Oxford, 2015; pp 418–463.
14. Rubenstein, D. I.; Koehl, M. A. R. *Am. Nat.* **1977**, 111(981), 981–994.
15. LaBarbera, M. *Am. Zool.* **1984**, 24, 71–84.
16. Jumars, P. A. *Concepts in biological oceanography. An interdisciplinary primer;* Oxford University Press: Oxford, 1993.
17. Vogel, S. *Life in moving fluids. The physical biology of flow.* Princeton University Press: Princeton, NJ, 1994.
18. Shimeta, J.; Koehl, M. A. R. *J. Exp. Mar. Biol. Ecol.* **1997**, 209, 47–73.
19. Rosenberg, G. G. *Limnol. Oceanogr.* **1980**, 25, 738–742.
20. Paffenhöfer, G. A.; Strickler, J. R.; Alcaraz, M. *Mar. Biol.* **1982**, 67, 193–199.
21. Wägele, J. W. *Phil. Trans. R. Soc. Lond. B* **1987**, 316, 429–458.
22. Gerritsen, J.; Porter, K. G.; Strickler, J. R. *Bull. Mar. Sci.* **1988**, 43(3), 366–376.

441 23. Hamner, W. M.; Hamner, P. P. *Can. J. Fish. Aquat.* **2000**, 57(S3), 192–202.
442 24. Garm, A.; Høeg, J. T. *Biol. Bull.* **2001**, 200(3), 281–297.
443 25. Garm, A.; Hallberg, E.; Høeg, J. T. *Biol. Bull.* **2003**, 204(2), 126–137.
444 26. Garm, A. *J. Morphol.* **2004**, 260(1), 85–100.
445 27. Gonçalves, R. J.; van Someren Gréve, H.; Couespel, D.; Kiørboe, T. *Mar. Ecol. Prog. Ser.* **2014**, 517,
446 61–74.
447 28. Giuffre, C.; Hinow, P.; Jiang, H.; Strickler, J. R. *Sci. Rep.* **2019**, 9, 17742.
448 29. Koehl, M. A. R.; Strickier, J. R. *Limnol. Oceanogr.* **1981**, 26(6), 1062–1073.
449 30. Gerritsen, J.; Porter, K. G. *Science* **1982**, 216(4551), 1225–1227.
450 31. Gophen, M.; Geller, W. *Oecologia* **1984**, 64, 408–412.
451 32. Ganf, G. G.; Shiel, R. J. *Mar. Freshw. Res.* **1985**, 36, 371–381.
452 33. Monger, B. C.; Landry, M. R. *Mar. Ecol. Prog. Ser.* **1990**, 65(2), 123–140.
453 34. Garm, A.; Høeg, J. T. *Mar. Biol.* **2000**, 137, 123–138.
454 35. Koehl, M. A. R. *J. Biomech.* **2004**, 37(6), 789–795.
455 36. Geierman, C.; Emlet, R. *J. Exp. Mar. Biol. Ecol.* **2009**, 379(1–2), 68–76.
456 37. Garm, A. *Mar. Biol.* **2005**, 147, 1179–1190.
457 38. Vittori, M.; Srot, V.; Bussmann, B.; Predel, F.; van Aken, P. A.; Štrus, J. *Micron* **2018**, 112, 26–34.
458 39. Cannon, H. G. *Brit. J. Exp. Biol.* **1929**, 6, 131–144.
459 40. Marshall, S. M.; Orr, A. P. *J. Mar. Biol. Assoc. UK* **1966**, 46, 513–530.
460 41. Boyd, C. M. *Limnol. Oceanogr.* **1976**, 21, 175–180.
461 42. Nival, P.; Nival, S. *Limnol. Oceanogr.* **1976**, 21, 24–38.
462 43. Nival, P.; Nival, S. *Limnol. Oceanogr.* **1979**, 24, 995–998.
463 44. Price, H. J.; Paffenhöfer, G. A. *Limnol. Oceanogr.* **1986**, 31, 189–194.
464 45. Hansen, B.; Tiselius, P. *J. Plankton Res.* 1992, 14, 821–834.
465 46. Kiørboe, T.; Saiz, E. *Mar. Ecol. Prog. Ser.* **1995**, 122, 135–145.
466 47. Kiørboe, T. *Sci. Mar.* **1997**, 61(Suppl. 1), 141–158.

48. Kiørboe, T. *A mechanistic approach to plankton ecology;* Princeton University Press: Princeton, NJ, 2008.
49. Jansen, S. Feeding behaviour of calanoid copepods and analyses of their faecal pellets. Ph. D. Thesis, Universität Bremen, Germany, 2006.
50. Tiselius, P.; Saiz, E.; Kiørboe, T. *Limnol. Oceanogr.* **2013**, 58(5), 1657–1666.
51. Kadiene, E. U.; Ouddane, B.; Hwang, J. S.; Souissi, S. *Sci. Rep.* **2019**, 9, 9492.
52. Michels, J.; Gorb, S. N. *J. Microsc.* **2012**, 245(1), 1–16.
53. Michels, J.; Gorb, S. N. *Beilstein J. Nanotechnol.* **2015**, 6, 674–685.
54. Michels, J. Confocal laser scanning microscopy – detailed three-dimensional morphological imaging of marine organisms. In *Imaging marine life: macrophotography and microscopy approaches for marine biology;* Reynaud, E. G., Ed.; Wiley-VCH: Weinheim, Germany, 2013; pp 69–91.
55. Peisker, H.; Michels, J.; Gorb, S. N. *Nat. Commun.* **2013**, 4, 1661.
56. Gorb, S. N. *Am. Entomol.* **2005**, 51(1), 31–35.
57. Gorb, S. N. *Phil. Trans. R. Soc. A.* **2008**, 366, 1557–1574.
58. Büscher, T. H.; Gorb, S. N. *Beilstein J. Nanotechnol.* **2021**, 12, 725–743.
59. Monaghan, J. J. *Comp. Phys. Comm.* **1988**, 48, 88–96.
60. Pöschel, T.; Schwager, T. *Computational granular dynamics: Models and algorithms;* Springer: Berlin, Germany, 2005.
61. Hoover, W. G. *Smooth particle applied mechanics. The state of the art,* vol. 25; Advanced Series in Nonlinear Dynamics, World Scientific, 2006.
62. Radjai, F.; Dubois, F. *Discrete-element modeling of granular materials;* Wiley-ISTE: London, 2011.
63. Dmitriev, A. I.; Nikonov, A. Y.; Filippov, A. E.; Psakhie, S. G. *Phys. Mesomech.* **2019**, 22, 375–381.
64. Filippov A. E.; Popov, V. L. *Facta Universitatis. Series: Mechanical Engineering* **2022**. doi.org/10.22190/FUME220327020F.